Applied Physics Letters

High magneto-Seebeck effect at room temperature in $Bi_{1.8}Sb_{0.2}Te_{3-y}Se_y$ crystal

Cite as: Appl. Phys. Lett. **118**, 243901 (2021); https://doi.org/10.1063/5.0053151
Submitted: 05 April 2021 • Accepted: 31 May 2021 • Published Online: 14 June 2021

P. K. Ghose, T. K. Dalui, A. Chatterjee, et al.

Applied Physics Letters ARTICLE scitation.org/journal/apl

High magneto-Seebeck effect at room temperature in $Bi_{1.8}Sb_{0.2}Te_{3-y}Se_y$ crystal

Cite as: Appl. Phys. Lett. **118**, 243901 (2021); doi: 10.1063/5.0053151
Submitted: 5 April 2021 · Accepted: 31 May 2021 ·
Published Online: 14 June 2021

P. K. Ghose, T. K. Dalui, A. Chatterjee, S. Majumdar, and S. Giri[a)]

AFFILIATIONS

School of Physical Sciences, Indian Association for the Cultivation of Science, Jadavpur, Kolkata 700032, India

[a)]Author to whom correspondence should be addressed: sspsg2@iacs.res.in

ABSTRACT

We report thermoelectric and electrical transport properties of $Bi_{1.8}Sb_{0.2}Te_{3-y}Se_y$ by tuning y. In contrast to the reported p-type conductivity of the end compounds with $y = 0$ and 3, a dominant n-type conduction mechanism is observed for $y = 1.5$ from the Hall measurement. Intriguingly, the magneto-Seebeck consequence is enhanced up to $\sim$ 20 times for $y = 1.5$ compared to the end members. The reasonable value of magnetoresistance with an anisotropic character with respect to the direction of the magnetic field is observed at low temperature, which decreases with increasing temperature. The density of state at the Fermi level near room temperature correlates high Seebeck coefficient as well as magneto-Seebeck effect. High magneto-Seebeck effect at room temperature is promising for the application.

High performance thermoelectric (TE) materials are the smart energy materials, which can efficiently convert the heat energy to the electrical energy.[1–8] In principle, plenty of available waste heat can be employed to generate electricity using the promising TE materials.[9–11] Practically, the promising TE materials have been proposed for efficient TE energy converters, such as refrigerators and thermostats.[12,13] Importantly, this technology is eco-friendly and does not emit pollutant, which relieves the global climate change. Therefore, exploring high TE materials and tuning of their TE properties by different parameters are desirable for the applications. Tuning of Seebeck (S) coefficient driven by the magnetic field (H) or magneto-Seebeck effect has been recently proposed as a promising technique in various systems, including magnetic tunnel junction,[14] charge ordered compound,[15] multilayer films involving giant magnetoresistance,[16] bismuth micro-wire,[17] Dirac semi-metal,[18] and topological insulators (TI).[19,20]

Topological insulators recently attract special attention for the advanced thermoelectric energy conversion and regulation of S with H, which has been attributed to the topological spin texture.[21] Interplay between the tuning of carrier concentration, manipulation of density of states, and the intricate phonon scattering has been proposed to lead the crucial role for high S in TI.[22] For example, hole doping in $Bi_{2-x}Sb_xTe_3$ has been recognized as a rich platform for tuning TE properties.[23,24] The n-type Bi_2Te_3 compound becomes p-type attributed to the hole doping in $Bi_{1.8}Sb_{0.2}Te_3$ and becomes promising TE material.[25,26] The optimization of the electronic properties has been further tuned by manipulating y in $Bi_{2-x}Sb_xTe_{3-y}Se_y$.[27–31] Although the studies of the TE properties have been attempted quite adequately on different TIs, tuning of the TE properties by the external parameters is rather less explored at room temperature, focusing on the applications.

In this Letter, we report efficient manipulation of S by the magnetic field or significant magneto-Secbeck effect at room temperature in $Bi_{1.8}Sb_{0.2}Te_{3-y}Se_y$ by tuning y. We note that the value of S is considerable as $\sim$ $-160\,\mu$V/K close to room temperature for $y = 1.5$. Intriguingly, we observe strong H dependence of S at room temperature. The change in S (ΔS) is promising up to $\sim$38 μV/K at 300 K for $H = 70$ kOe. We note that Hall mobility is strongly influenced by the y-values, where the n-type charge carrier mainly dominates for $y = 1.5$, in contrast to that reported p-type conduction mechanism for the end members with $y = 0$ and 3. A reasonable magnetoresistance (MR) is observed, which is anisotropic in character with respect to the direction of H. The charge carrier densities and MR have been correlated with promising magneto-Seebeck effect.

Single crystals of $Bi_{1.8}Sb_{0.2}Te_{3-y}Se_y$ (BSTS) with $y = 0$, 1.5, and 3 are grown using the modified Bridgman method.[31] The shiny silver-colored single crystals are obtained with a maximum area of $\sim$3 $\times$ $\sim$2 mm. The phase purity is initially determined at 300 K for both the powder and crystals by the x-ray diffraction (XRD) technique using Cu-Kα radiation in a PANalytical X'Pert PRO diffractometer. Synchrotron diffraction studies are further carried out at low temperatures in the range of 10–300 K with a wavelength of 0.14235 Å

(87.1 keV) at the P07 beamline of PETRA III, Hamburg, Germany, using a 2D Perkin Elmer detector. The analysis of these synchrotron powder diffraction data is done using Rietveld refinement with a commercially available MAUD software. High resolution transmission electron microscopy (HRTEM) is performed by using a JEOL TEM 2010. Energy dispersive x-ray spectroscopy (EDS) is performed in a JEOL JSM-6010LA scanning electron microscope (SEM) to confirm the composition and the homogeneity of the single crystal. X-ray photoemission spectroscopy (XPS) is recorded with a spectrometer of O micrometer Nanotechnology. The Seebeck coefficient is measured using a home built setup coupled to the multifunctional probe of the PPMS system of Quantum Design (PPMS-II).[32] Electrical transport measurements are done in the same system (PPMS II, Quantum Design) using the standard four-probe technique.

Here, detailed investigations are carried out mainly for the BSTS single crystal with $y = 1.5$. The powder x-ray diffraction (XRD) studies are performed on the fine powder of the crashed crystal at 298 K. The XRD pattern is depicted in Fig. 1(a) for $y = 1.5$. The continuous curve shows the Rietveld refinement using the $R\bar{3}m$ space group, which is consistent with the previous reports.[27–29] The bars depict the diffraction peak positions, whereas the difference plots shown below the diffraction patterns confirms the phase purity and indicates the absence of any unidentified phase. The lattice constants are obtained to be $a = 4.3848(1)$, $c = 30.5065(5)$ Å. The refined coordinates are Bi [0,0,0.4027(2)], Sb [0,0,0.4027(2)], Te1 [0,0,0.1966(4)], Te2 (0,0,0), Se1 [0,0,1966(4)], and Se2 (0,0,0) with the reliability parameters, R_w (%) = 4.69, R_{exp} (%) = 2.80, and $\chi^2 = 1.67$. Figure 1(b) depicts the XRD patterns of the crystals along the planes parallel to the (003) plane. The sharp peaks confirm reasonably good crystalline nature. Insets of Figs. 1(a) and 1(b) illustrate the selected area electron diffraction (SAD) pattern and HRTEM image, showing a clean image of a (012) plane. The periodic pattern of the spots in the SAD image demonstrates the (012) and (113) planes and further implies the high quality of the crystal. The refined lattice constants a and c, as obtained from the refinement, are plotted with temperature, which are shown in Fig. 1(c). Both the lattice constants, a and c, decrease linearly with the decreasing temperature until ∼75 K, below which they decrease slowly with further decreasing temperature.

Kelvin probe force microscopy is used to determine the work function. Figure 1(d) exhibits the contact potential difference (CPD) mapped on the surface of the crystal with respect to a highly oriented pyrolytic graphite (HOPG), where inset shows the contact potential image. A straight line on the image guides the direction of mapping on the surface. By taking into account of the work function of HOPG, the value of work function of the BSTS crystal with $y = 1.5$ is found to be 4.81 eV. The value is much smaller than pristine Bi_2Te_3 (5.25) and Bi_2Se_3 (5.60 eV),[27] pointing that an upward shift of the chemical potential leads to the reduction of the work function. The XPS images of Bi, Sb, Se, and Te are shown in Figs. 1(e)–(h), respectively, where the deconvoluted components are obtained from the 4 $f_{7/2}$ and 4 $f_{5/2}$ contributions for Bi, and 3 $d_{5/2}$ and 3 $d_{3/2}$ contributions for rest of the elements. The deconvoluted components are shown by the continuous curves. Using the XPS, one can determine the composition between the elements. For example, the ratio between Se and Te can be expressed as $\rho_{Se}/\rho_{Te} = (I_{Se}/S_{Se})/(I_{Te}/S_{Te})$. Here, ρ is the atomic density, I is the integrated peak intensity, as obtained from the area under the deconvoluted curve, and S is the atomic sensitivity factor.[33] Considering the available values of S_{Bi}, S_{Sb}, S_{Se}, and S_{Te} from the literature,[34] the values of ρ_{Bi}/ρ_{Sb}, ρ_{Bi}/ρ_{Te}, ρ_{Bi}/ρ_{Se}, and ρ_{Te}/ρ_{Se} are 9.136, 1.193, 1.185, and 0.994, respectively, which provides the ratio of Bi:Sb:Te:Se to be 1.780:0.196:1.505:1.517. The ratio is found to be close to 1.790:0.195:1.495:1.527, respectively, for Bi:Sb:Te:Se, as obtained from the SEM EDS, which is also close to the desired composition.

The resistivity (ρ_{xx}) is measured in field and with H applied parallel (||) and perpendicular (⊥) to the crystallographic c-axis. Here, the suffix "xx" points to the direction of current and measured voltage in the same direction. Here, the direction of H for the || and ⊥ component of ρ_{xx} is always ⊥ to the direction of current. Initially, $\rho_{xx}(T)$ [left axis] decreases with decreasing T and it increases below ∼80 K, displaying a minimum for the measurement in zero-field, as

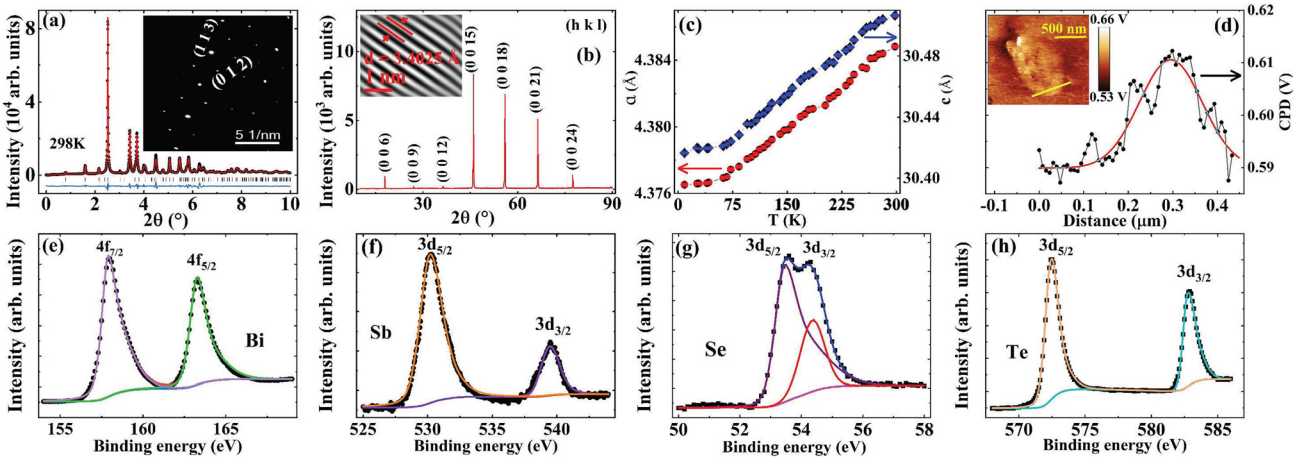

FIG. 1. X-ray (a) powder diffraction patterns (symbols) with Rietveld refinement (solid curves) and (b) diffraction pattern of a single crystal along the planes parallel to the (003) plane at 298 K. Insets of (a) and (b) depict SAD pattern and HRTEM image, respectively. T variations of lattice constants (c) a and c. (d) Mapping of contact potential difference (CPD) on the crystal surface with respect to HOPG and contact potential image (inset). XPS images of (e) Bi, (f) Sb, (g) Se, and (h) Te for $Bi_{2-x}Sb_xTe_{3-y}Se_y$ with $x = 0.2$ and $y = 1.5$.

shown in Fig. 2(a). In field, the positive magnetoresistance (MR) emerges, as shown by the increase in ρ_{xx}. The || and ⊥ components of ρ_{xx} are shown by the continuous and broken curves, respectively. Both the || and ⊥ components of MR [right axis], defined as $[\rho_{xx}(H) - \rho_{xx}(H=0)]/\rho_{xx}(H=0)$, are depicted with T in Fig. 2(a). The MR-H curves at different T are shown in Fig. 2(b). The value of MR of the || component is reasonable as ∼23 at 2 K and for $H = 90$ kOe. The || component of MR is always larger than the ⊥ component in the high-H regime, whereas it is opposite below ∼65 kOe. Current investigation is not sufficient enough to predict the nature of the Fermi surface (FS). However, similar results have been occasionally observed in topological semi-metals, proposing the anisotropic FS from the direction dependent MR results.[35–37] Here, BSTS single crystal with $y = 1.5$ exhibits semi-metallic character. Here, we do not observe any Shubnikov-de Haas oscillation for characterizing topological insulating character until the measurement of 90 kOe. The amplitude of the Shubnikov-de Haas oscillations is damped exponentially with decreasing magnetic field.[38] The damping may be attributed to both disorder broadening of the Landau levels and thermal spread of the Fermi function, which is predominant until 90 kOe for $y = 1.5$. Nevertheless, the topological insulating properties may be identified from their response to an electromagnetic field.[39] Under the proper conditions, TIs have a universal quantized magnetoelectric response coefficient $e^2/2h$. However, it is quite difficult to achieve the response in real materials that can have disorder, finite chemical potential, and residual dissipation factor.

To probe the carrier concentration (n_e) and mobility (μ_e), the resistivity is recorded in the Hall geometry, where the ρ_{yx} is defined as $\rho_{yx} = (V_y/I_x)t$, t (here, $t = 0.05$ mm) being the thickness of the sample, and V_y being the transverse voltage in H, recorded along the ⊥ direction to I_x. The linear $\rho_{yx} - H$ is depicted in the inset of Fig. 2(c) at selected T, pointing to a dominant single charge carrier. The analysis of the $\rho_{yx} - H$ curve pzrovides $n_e(T)$ and $\mu_e(T)$, which are shown in Figs. 2(c) and 2(d), respectively, as a function of T. Initially, $n_e(T)$ decreases slowly with increasing T, which is followed by another rapid decrease above ∼200 K. $\mu_e(T)$ increases initially; then, it becomes flat above ∼75 K, and a sharp rise in μ_e is observed close to room temperature.

Thermoelectric properties with T and H are investigated along the crystallographic c-axis. The values of S with T are depicted in the inset of Fig. 3(a). The values of S are always negative, pointing a dominant electron conduction, which is consistent with the Hall results. With increasing T, the $|S|$ increases with increasing T and the value of $|S|$ is considerably large as ∼160 μV/K at 300 K, which is comparable to those for n-type Bi_2Se_3[40] and Bi_2Te_3.[41] We further note that the values of S are +13.5 and +9.5 μV/K, respectively, at 300 K. The value of $|S|$ is correlated with the carrier density (n) for the highly degenerate electron gas, following the proposed Mott–Jones relation as $S = \frac{\pi^2 K_B^2 T}{3q}\left[\frac{d\ln\sigma(E)}{dE}\right]_{E=E_F}$, where σ is the conductivity, $q = \pm e$ (hole/electron).[42] The value of S correlates the term in the third bracket, where the density of state at the Fermi level leads a significant role.[43] The role of charge scattering anisotropy on the thermoelectric properties is another important parameter, which has been discussed in the $(Bi,Sb)_2(Te,Se,S)_3$ solid solutions.[44] Here, the change in n-type charge scattering anisotropy due to fractional substitution of Se atoms in the BSTS may lead significant role on tuning the value of S for $y = 1.5$.

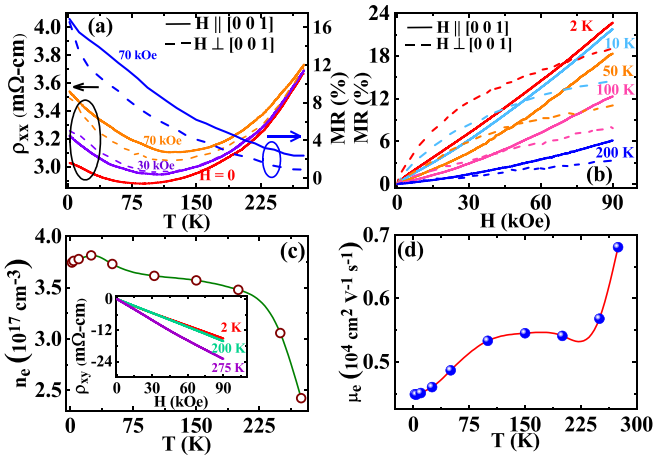

FIG. 2. (a) T variations of || and ⊥ components of ρ_{xx} (left axis) for $H = 0$, 30, and 70 kOe and MR (right axis) at 70 kOe. (b) || and ⊥ components of MR–H curves at selected T. T variations of (c) n_e and (d) μ_e. Inset of (c) depicts ρ_{yx} curves with H for for $Bi_{1.8}Sb_{0.2}Te_{3-y}Se_y$ with $y = 1.5$.

Figure 3(a) depicts the H dependence of change in S, defined as $\Delta S/S = [S(H) - S(H=0)]/S(H=0)$ at selected T. The value of $|\Delta S/S|$ increases with H as well as T. Here, the maximum value of $|\Delta S/S|$ is observed to be ∼24% at 300 K for $H = 70$ kOe. Considering

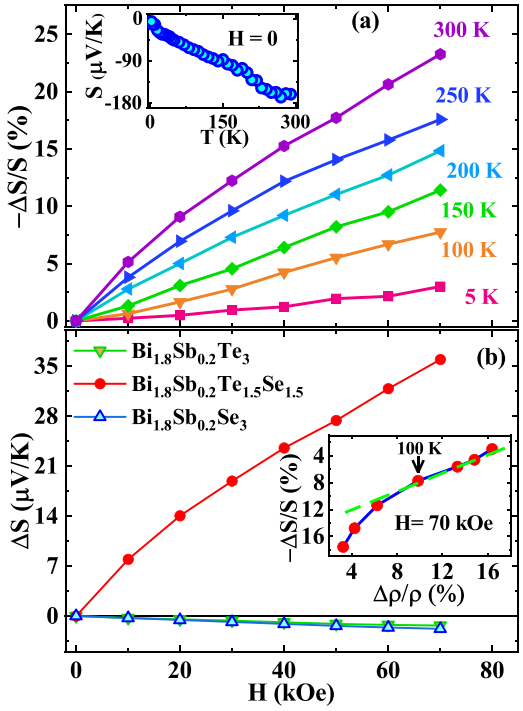

FIG. 3. (a) $\Delta S/S$ with H at selected T for $Bi_{1.8}Sb_{0.2}Te_{3-y}Se_y$ with $y = 1.5$. Inset of (a) depicts T variation of S at $H = 0$. (b) ΔS with H at 300 K for $y = 0$, 1.5, and 3.0. Inset of (b) depicts the plot of $\Delta\rho/\rho$ with $\Delta S/S$ for different temperatures at $H = 70$ kOe. Linearity of the plot below ∼100 K is indicated by the broken straight line.

the diffusion mechanism of a single band metal with the n-type carrier, the H dependence of S is given by the Mott relationship,[45,46] $S(H) = \alpha[(\sigma^2\beta + \sigma_{xy}^2\gamma)/(\sigma^2 + \sigma_{xy}^2)]$ with $\sigma = ne\mu$, $\sigma_{xy} = ne\mu^2 H$, $\alpha = \pi^2 k_B^2 T/3e$, $\beta = \partial \ln \sigma/\partial\zeta$, and $\gamma = \partial \ln \sigma_{xy}/\partial\zeta$ with ζ being a chemical potential. Here, the H dependence of $S(H)$ is influenced by the σ_{ij}. A strong correlation between MR and $\Delta S/S$ has been discussed in few systems, such as $Ag_{2-\delta}Te$,[47] $Sb_{2-x}Sn_xTe_3$,[32] and Sb_2Te_2Se.[48] Inset of Fig. 3(b) depicts the values of $\Delta\rho/\rho$ with $-\Delta S/S$ for $H = 70$ kOe at different temperatures, where H in both the measurements is applied along the [001] direction. Linearity of the plot is indicated by the broken straight line below ~100 K, where MR is more than ~10%. The results may indicate that the $-\Delta S/S$ may be correlated with $\Delta\rho/\rho$ below ~100 K. However, it does not hold at higher temperature, where $|\Delta S/S|$ is higher and MR is lower in magnitude. Adequate experimental investigations with proper theoretical understanding of the magneto-Seebeck consequence need to be explored to understand the underline mechanism. Figure 3(b) depicts ΔS with H at 300 K for $y = 1.5$, which is compared with the results of the crystals for $y = 0$ and 3, exhibiting contrast behavior. The value of ΔS at 300 K for $H = 70$ kOe is considerable as ~38 μV/K for $y = 1.5$. Remarkably, the value of $|\Delta S|$ is ~20 times larger than the values for $y = 0$ and 3. The results indicate that the doping at y is crucial for tuning the magneto-Seebeck coefficient in $Bi_{1.8}Sb_{0.2}Te_{3-y}Se_y$, where large magneto-Seebeck effect is observed with the n-type conduction mechanism in contrast to the p-type conductivity observed for the end compounds.[49]

In conclusion, a large magneto-Seebeck effect is observed for n-type $Bi_{1.8}Sb_{0.2}Te_{1.5}Se_{1.5}$, which is ~20 times higher than the end compounds having p-type conductivity. Magnetoresistance of BSTS ($y = 1.5$) is reasonable, which relates linearly to the magneto-Seebeck effect at low temperature. Current investigation proposes that Seebeck coefficient can be efficiently manipulated by the magnetic field at room temperature, which attracts the community for the applications.

Portions of this work were carried out at the light source PETRA III of DESY, a member of the Helmholtz Association (HGF). Financial support (Proposal No. I-20170178) by the Department of Science & Technology (Government of India) provided within the framework of the India@DESY collaboration is gratefully acknowledged. The authors acknowledge Mr. R. Chakraborty for performing experiment on Kelvin Probe Force Microscopy. The authors would like to thank Professor A. J. Pal for the discussions.

S.G. and P.K.G conceived the idea. P.K.G. and T.K.D. designed the experiment. P.K.G. fabricated the crystal. P.K.G. and T.K.D. performed all the experiments except for the synchrotron diffraction studies, which was performed by A.C. All the analysis was performed by P.K.G. and S.G. wrote the manuscript. All authors participated in the discussion of the results and corrected multiple iterations of the manuscript.

DATA AVAILABILITY

The data that support the findings of this study are available from the corresponding author upon reasonable request.

REFERENCES

[1]C. D. Stow, Rep. Prog. Phys. **32**, 1 (1969).
[2]C. C. Wood, Rep. Prog. Phys. **51**, 459 (1988).
[3]T. Inohara, Y. Okamoto, Y. Yamakawa, A. Yamakage, and K. Takenaka, Appl. Phys. Lett. **110**, 183901 (2017).
[4]M. Y. Swinkels and I. Zardo, J. Phys. D: Appl. Phys. **51**, 353001 (2018).
[5]T. Tan, L.-D. Zhao, and M. G. Kanatzidis, Chem. Rev. **116**, 12123 (2016).
[6]J. C. Caylora, K. Coonley, J. Stuart, T. Colpitts, and R. Venkatasubramanian, Appl. Phys. Lett. **87**, 023105 (2005).
[7]D. Narducci, Appl. Phys. Lett. **99**, 102104 (2011).
[8]J. Zhou, H. Zhu, T.-H. Liu, Q. Song, R. He, J. Mao, Z. Liu, W. Ren, B. Liao, D. J. Singh, Z. Ren, and G. Chen, Nat. Commun. **9**, 1721 (2018).
[9]F. J. DiSalvo, Science **285**, 703 (1999).
[10]M. E. Kiziroglou, A. Elefsiniotis, S. W. Wright, T. T. Toh, P. D. Mitcheson, T. Becker, and E. M. Yeatman, Appl. Phys. Lett. **103**, 193902 (2013).
[11]X. Zianni, Appl. Phys. Lett. **97**, 233106 (2010).
[12]H. J. Goldsmid, *Electronic Refrigeration* (Pion, London, 1986).
[13]M. Nesarajah and G. T. Frey, Mater. Today **5**, 10283 (2018).
[14]J. M. Teixeira, J. D. Costa, J. Ventura, M. P. Fernandez-Garcia, J. Azevedo, J. P. Araujo, J. B. Sousa, P. Wisniowski, S. Cardoso, and P. P. Freitas, Appl. Phys. Lett. **102**, 212413 (2013).
[15]D. V. Maheswar Repaka and R. Mahendiran, Appl. Phys. Lett. **103**, 162408 (2013).
[16]X. K. Hu, P. Krzysteczko, N. Liebing, S. Serrano-Guisan, K. Rott, G. Reiss, J. Kimling, T. Böhnert, K. Nielsch, and H. W. Schumacher, Appl. Phys. Lett. **104**, 092411 (2014).
[17]Y. Hasegawa, Y. Ishikawa, T. Komine, T. E. Huber, A. Suzuki, H. Morita, and H. Shirai, Appl. Phys. Lett. **85**, 917 (2004).
[18]H. Wang, X. Luo, K. Peng, Z. Sun, M. Shi, D. Ma, N. Wang, T. Wu, J. Ying, Z. Wang, and X. Chen, Adv. Funct. Mater. **29**, 1902437 (2019).
[19]Y. Fujishiro, N. Kanazawa, T. Shimojima, A. Nakamura, K. Ishizaka, T. Koretsune, R. Arita, A. Miyake, H. Mitamura, K. Akiba, M. Tokunaga, J. Shiogai, S. Kimura, S. Awaji, A. Tsukazaki, A. Kikkawa, Y. Taguchi, and Y. Tokura, Nat. Commun. **9**, 408 (2018).
[20]C. Fu, S. N. Guin, T. Scaffidi, Y. Sun, R. Saha, S. J. Watzman, A. K. Srivastava, G. Li, W. Schnelle, S. S. P. Parkin, C. Felser, and J. Gooth, Research **2020**, 4643507.
[21]B. Skinner and L. Fu, Sci. Adv. **4**, eaat2621 (2018).
[22]C. Fu, Y. Sun, and C. Felser, APL Mater. **8**, 040913 (2020).
[23]X. He, T. Guan, X. Wang, B. Feng, P. Cheng, L. Chen, Y. Li, and K. Wu, Appl. Phys. Lett. **101**, 123111 (2012).
[24]J. Kellner, M. Eschbach, J. Kampmeier, M. Lanius, E. Mlyńczak, G. Mussler, B. Holländer, L. Plucinski, M. Liebmann, D. Grützmacher, C. M. Schneider, and M. Morgenstern, Appl. Phys. Lett. **107**, 251603 (2015).
[25]N. T. Huong, Y. Setou, G. Nakamoto, M. Kurisu, T. Kajihara, H. Mizukami, and S. Sano, J. Alloys Compd. **368**, 44 (2004).
[26]H.-J. Im, D.-H. Kim, J.-S. Ahn, H. Iwasaki, S. Sano, K.-C. Je, and T. Mitani, Jpn. J. Appl. Phys. Part 1 **43**, 3548 (2004).
[27]D. Takane, S. Souma, T. Sato, T. Takahashi, K. Segawa, and Y. Ando, Appl. Phys. Lett. **109**, 091601 (2016).
[28]Z. Ren, A. A. Taskin, S. Sasaki, K. Segawa, and Y. Ando, Phys. Rev. B **84**, 165311 (2011).
[29]T. Arakane, T. Sato, S. Souma, K. Kosaka, K. Nakayama, M. Komatsu, T. Takahashi, Z. Ren, K. Segawa, and Y. Ando, Nat. Commun. **3**, 636 (2012).
[30]P. Mal, B. Das, G. Bera, P. Rambabu, G. R. Turpu, C. V. Tomy, and P. Das, J. Appl. Phys. **129**, 095702 (2021).
[31]P. K. Ghose, T. K. Dalui, and S. Giri, AIP Conf. Proc. **2265**, 030423 (2020).
[32]T. K. Dalui, P. K. Ghose, S. Majumdar, and S. Giri, J. Phys.: Condens. Matter **32**, 435601 (2020).
[33]G. Zhang, H. Qin, J. Teng, J. Guo, Q. Guo, X. Dai, Z. Fang, and K. Wu, Appl. Phys. Lett. **95**, 053114 (2009).
[34]C. D. wagner, J. Electron Spectrosc. Relat. Phenom. **32**, 99 (1983).
[35]M. N. Ali, J. Xiong, S. Flynn, J. Tao, Q. D. Gibson, L. M. Schoop, T. Liang, N. Haldolaarachchige, M. Hirschberger, N. P. Ong, and R. J. Cava, Nature **514**, 205 (2014).
[36]S. N. Zhang, Q. S. Wu, Y. Liu, and O. V. Yazyev, Phys. Rev. B **99**, 035142 (2019).
[37]N. J. Ghimire, M. A. Khan, A. S. Botana, J. S. Jiang, and J. F. Mitchell, Phys. Rev. Mater. **2**, 081201(R) (2018).
[38]I. M. Lifshitz and L. M. Kosevich, Sov. Phys. JETP **6**, 67 (1958).
[39]D. Culcer, A. C. Keser, Y. Li, and G. Tkachov, 2D Mater. **7**, 022007 (2020).

[40]Y. S. Hor, A. Richardella, P. Roushan, Y. Xia, J. G. Checkelsky, A. Yazdani, M. Z. Hasan, N. P. Ong, and R. J. Cava, Phys. Rev. B **79**, 195208 (2009).
[41]J. H. Dennis, Adv. Energy Convers. **1**, 99 (1961).
[42]H. Fritzsche, Solid State Commun. **9**, 1813 (1971).
[43]N. F. Mott and H. Jones, *The Theory of the Properties of Metals and Alloys* (Dover Publications, New York, 1958).
[44]L. N. Lukyanova, V. A. Kutasov, P. P. Konstantinov, and V. V. Popov, Phys. Solid State **50**, 597 (2008).
[45]R. D. Barnard, *Thermoelectricity in Metals and Alloys* (Taylor & Francis, London, 1972).
[46]T. Liang, Q. Gibson, J. Xiong, M. Hirschberger, S. P. Koduvayur, R. J. Cava, and N. P. Ong, Nat. Commun. **4**, 2696 (2013).
[47]Y. Sun, M. B. Salamon, M. Lee, and T. F. Rosenbaum, Appl. Phys. Lett. **82**, 1440 (2003).
[48]K. Wang, D. Graf, and C. Petrovic, Phys. Rev. B **89**, 125202 (2014).
[49]P. K. Das, T. J. Whitcher, M. Yang, X. Chi, Y. P. Feng, W. Lin, J. S. Chen, I. Vobornik, J. Fujii, K. A. Kokh, O. E. Tereshchenko, C. Z. Diao, J. Moon, S. Oh, A. H. Castro-Neto, M. B. H. Breese, A. T. S. Wee, and A. Rusydi, Phys. Rev. B **100**, 115109 (2019).